



Silk fibroin molecularly imprinted nanoparticles as biocompatible molecular nanotraps: Molecular recognition ties the knot with biomaterials. The bioMIP's labeling and degradation

Devid Maniglio¹ · Francesca Agostinacchio¹ · Alessandra Maria Bossi²

Received: 11 November 2022 / Accepted: 18 January 2023
© The Author(s) 2023

Abstract

Molecularly imprinted nanoparticles (nanoMIPs) are biomimetic polymeric nanomaterials, typically prepared from acrylamide and derivatives, that are formed by a template-assisted synthesis. NanoMIPs display high affinity, selectivity, and specificity for the targeted molecule, on the par of natural receptors and antibodies. Recently, we introduced a paradigmatic change by forming nanoMIPs starting from biomaterials, under the name of bioMIPs, as a strategy to promptly translate them into the clinical settings. Silk fibroin, that is a biocompatible and non-immunogenic natural material, was used as a building block for the synthesis of bioMIPs tailored to recognize the protein human serum albumin. BioMIPs confirmed high selectivity and specificity for the targeted protein, together with cytocompatibility. The present work expands the actual knowledge on bioMIPs, studying a route to post-synthetically entail fluorescent tags, with the aim to localize these molecular nanotraps in cells and tissues. Moreover, the enzymatic degradation of bioMIPs was investigated, to support the role of bioMIPs as greener and biocompatible alternatives to non-natural biomimetics.

Introduction

Biomaterials owning molecular recognition functions are expected to play a central role in the development of the next generation of therapeutics and instructive scaffolds. Among the techniques to prepare functional materials, there is the molecular imprinting of polymers (MIPs) [1]. MIPs are prepared by a template-assisted synthesis in which the targeted molecule acts as a template and is solvated together with monomers (typically acrylamides, acrylates, methacrylates monomers). The polymerization process embeds in the forming polymeric network molecular cavities that are stereochemically complementary to the template and therefore are able to rebind it. MIPs display affinity, specificity, and

selectivity for the targeted molecule on the par of the natural counterparts (antibodies, receptors). Advantages of the MIPs are the possibility to tune the recognition, by varying the mix of monomers [2]; the robustness, the processability typical of polymers; the easy and cheap synthesis and the possibility of reuse. Additionally, MIPs can be synthesized of nanometer dimensions (nanoMIPs) [3–5], rivaling with natural monoclonal antibodies [6]. NanoMIPs have been demonstrated to play functional roles *in vitro* and *in vivo* [7], such as disrupting cancer cells signal transmission [8], inhibiting cell adhesion [9], and removing toxins [3]. Thus, nanoMIPs hold great promises for applications in medicine, a domain in which the requirements of non-toxicity and biocompatibility are non-negotiable.

Despite *in vitro* tests indicated the non-toxicity of nanoMIPs [10], extensive studies should be performed to address the safety concerns on specific organ accumulation and on *in vivo* degradation. It is expected that developing a method to produce biological MIP nanoparticles, tailored to selectively bind a targeted analyte, but possessing the required biocompatibility, is crucial for the direct translation of nanoMIPs to clinical settings. For this, recently, we came up with the idea to synthesize fully biocompatible nanoMIPs starting from the natural polymer silk fibroin (SF), that is renowned for its biocompatibility and it is a

✉ Alessandra Maria Bossi
alessandramaria.bossi@univr.it

Devid Maniglio
devid.maniglio@unitn.it

¹ Department of Industrial Engineering, BIOtech Research Center, University of Trento, Via Delle Regole 101, Mattarello, 38123 Trento, Italy

² Molecular Imprinting Lab., Department of Biotechnology, University of Verona, Strada Le Grazie 15, 37134 Verona, Italy

promising material for Tissue Engineering and Regenerative Medicine (TERM). These new MIPs biomimetics have been named “bioMIPs” [11, 12]. The process of bioMIP formation is schematized in Fig. 1.

SF is a building block with interesting properties for the imprinting process. First of all, the SF polypeptide chains have a strong propensity for the beta structure; this latter in turn drives the spontaneous assembly of SF in a network of entangled fibers that form the basis of the bioMIP’s supramolecular nanostructure. Then, SF can be chemically functionalized with pendant double bonds [13], this has the advantage to crosslink the bioMIP’s, thus improving the stability of the nanoparticle and preserving the stereochemistry of the imprinted binding site. Finally, the amino acid sequence of SF offers chemical functionalities to maximize the template/monomer molecular pairing during the imprinting process, hence permitting to form high-affinity binding sites.

We have demonstrated the feasibility of the SF imprinting, both using a serum protein [12] and a peptide hormone [13] as templates, thus proving the possibility to imprint bioMIPs with both small and large molecular targets. In the present work, we investigate further the bioMIP, by studying the possibility to entail fluorescence to the bioMIPs, via post-synthetic tagging, with the final aim to map the bioMIPs distribution in cells cultures and tissues. Moreover, we studied whether bioMIPs underwent enzymatic degradation, in order to collect initial evidence on their biological elimination path.

Materials and methods

Synthesis of bioMIPs

Extraction and purification of silk fibroin (SF) were conducted as reported [14]. Fibroin-MA (SilMA) was prepared following [15]. Then, SilMA was adjusted to 0.3% w/v in

10 mM PB pH 7.4 buffer in the presence of the template (3 nmol human serum albumin, Sigma Aldrich). The final volume was 4 mL. Lithium phenyl-2,4,6-trimethylbenzoylphosphinate (LAP) was added at the final concentration of 0.2% w/w and polymerized for 1 min with a UV-LED light ($\lambda = 365$ nm, 4W). Then, the template was removed by the addition of Trizma free base to the bioMIP suspension, to reach pH of 10 and extensive dialysis under stirring, final dialysis in PBS. Protein removal was controlled by SDS-PAGE electrophoresis.

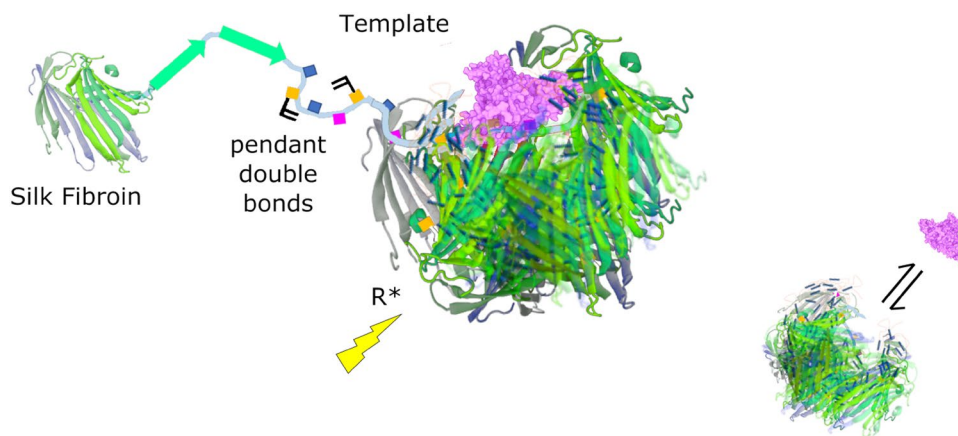
Dynamic light scattering

Size distribution and polydispersity index (PDI) of the bioMIPs were determined by Dynamic Light Scattering (DLS) using a Zetasizer Nano ZEN3600 (Malvern Instruments Ltd, Worcestershire, UK) equipped with a 633 nm He-Ne laser. BioMIPs were dispersed in filtered deionized water at 1 mg/mL and filtered 0.22 μ m prior to measurement. The material refractive index (RI) was 1.490 and the absorption value 0.01; the dispersant RI was 1.332, and the viscosity was 0.89 cP as reported by the Zetasizer v.6.32 software (Malvern instruments Ltd, Worcestershire, UK). The temperature was set at 298 K and a detection angle of 173° was used. Measurements were collected in triplicate. Untagged and Nile-Red and Rhodamine-tagged bioMIPs distributions were compared and analyzed for significance using Student’s *T* test.

Fluorescent decoration of bioMIPs

Rhodamine-bioMIPs were prepared with acryloxyethyl thio-carbamoyl rhodamine B (Sigma Aldrich, Darmstadt, Germany). The fluorescent dye (stock solution 0.02% w/v in DMSO) was added to the bioMIPs (850 μ g; $M_n \sim 9$ MDa) in molar excess (100:1 mol:mol). A volume of 20 μ L of LAP (1% w/v) was added to the solution, and photografting was triggered by exposing the solution for 1 min to UV-LED

Fig. 1 The concept of bioMIP. The source of biomaterials was silk, a natural polymer composed of two main proteins: sericin and fibroin. Silk fibroin (SF), that is a protein with a beta-fold, was methacrylated to provide pendant double bonds and exploited as building block to form “natural” MIP nanoparticles: the bioMIPs. As a template, the protein human serum albumin (pink) was chosen



light. At the end of the grafting, Rhoda-bioMIPs were extensively dialyzed to remove non-reacted tags. Alternatively, Nile-Blue-bioMIPs were prepared in a same manner, except for using the Nile-blue acrylamide (Polysciences, US) as fluorescent tag. The incorporation of the tag was controlled by measuring the fluorescent intensity of both the Rhoda- and the Nile-Blue- bioMIPs performing the measures on a Tecan Infinite PRO 200 spectrofluorometer for microplates (Tecan Lifesciences, Switzerland) in triplicate, using 96 Flat Bottom Black Polystyrene microtiter plates (Nunc™ MicroWell™ 96-Well, Nunclon Delta-Treated, Thermo Scientific, Germany). The excitation for Rhoda-bioMIPs was at the $\lambda_{exc} = 488$ nm and emission was recorded in the range 514–540 nm. The excitation for Nile-Blue-bioMIPs was at the $\lambda_{exc} = 633$ nm and emission was recorded in the range 645–740 nm. The calibration curve for acryloxyethyl thiocarbonyl rhodamine B in the range 1.2×10^{-12} to 1.2×10^{-9} M was y (Int. Em) = $7.88x + 30.806$, $R^2 = 0.999$. The calibration curve for Nile-blue acrylamide in the range 0.98×10^{-12} to 0.98×10^{-9} M was y (Int. Em) = $14.305x - 4.1933$, $R^2 = 0.999$.

In vitro cell culture in the presence of bioMIPs

For the in vitro experiments, human lung fibroblasts (MRC5—ATCC) were used at passage 18. The cells were seeded in a 96 well plate at a density of 1×10^5 cell/mL and cultured in expansion medium composed of MEM medium (Euroclone), supplemented with Fetal Bovine Serum (FBS—Euroclone) 10%, non-essential amino acids (Sigma Aldrich), Sodium pyruvate (Gibco), and antibiotic/antimycotic (Euroclone) 1%. After seeding, the cells were expanded for 24 h. NPs were then added to the wells at two different concentrations: 0.5 mg/mL and 0.1 mg/mL. All the samples were tested at 24 and 48 h after the NPs addition.

Confocal analysis

Cell adhesion and morphology, as well as bioMIPs' distribution were evaluated by laser scanning confocal microscopy (LSCM, Nikon A1—Japan). For each time point (24 and 48 h), two replicates for each condition were analyzed. Before confocal observations, samples were fixed with 4% paraformaldehyde (PFA—Sigma Aldrich) solution and incubated at room temperature (RT) for 20 min, then washed twice in PBS. Cell membranes were then permeabilized with Triton X (SigmaAldrich) 0.2% (v/v) solution and incubated for 20 min at RT. Nuclei and cytoskeleton staining was performed by adding 4',6-diamidino-2-phenylindole (DAPI—Sigma Aldrich) and Rhodamine Phalloidin (Thermo Fisher) according to the manufacturer's instructions, respectively. The samples were incubated protected from light exposure for 20 min at RT and then analyzed by LSCM using specific excitation wavelengths for cell nuclei and cytoskeleton

(405 nm and 561 nm) and for bioMIPs (636 nm), and collecting emission at 450/50 nm, 593/46 nm, and 700/38 nm, respectively.

Enzymatic degradation of bioMIPs

BioMIPs (1 mg/mL) were suspended in Tris–HCl at pH 8.2 and added either of the digesting enzyme trypsin (100 μ g) or of the enzyme Proteinase K (100 μ g). The digestion was run overnight at 37 °C. At the end of the digestion, samples were measured at DLS. Moreover, the digested bioMIP's samples were microcentrifuged on cellulose microfilters with MWCO 10,000 Da (Amicon) for 10 min at 8000 rpm. Centrifuged peptides were tested for fluorescent emission, as reported above.

Results and discussion

Fluorescent tagging of bioMIPs

BioMIPs were synthesized starting from methacrylated SF (SilMA). The SilMA building blocks were placed in buffer in the presence of the template, i.e., the protein human serum albumin (HSA) (Fig. 1). Photopolymerization stabilized the supramolecular SF nano-assemblies around the template, thus forming the bioMIPs, as reported in [11]. The bioMIPs hydrodynamic size, estimated by DLS (Fig. 2), reported a bioMIP population with a mean diameter (Z_{ave}) of 95.6 ± 1.2 nm and a polydispersity index (PDI) of 0.358.

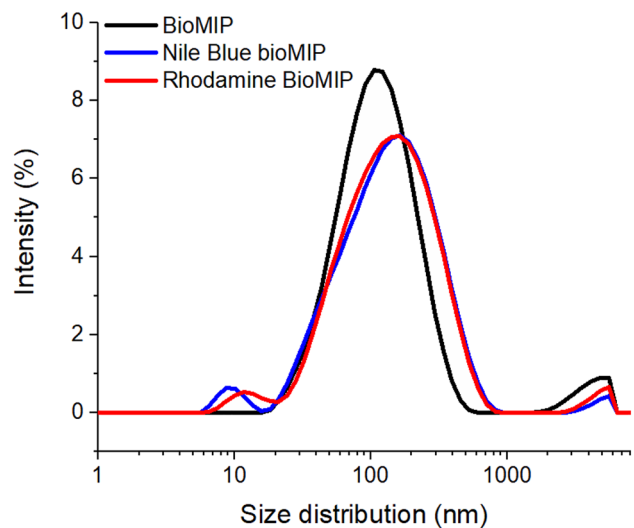


Fig. 2 Effect on the bioMIP's hydrodynamic size of the fluorescent tagging. DLS measurements showed the size distribution of the non-tagged bioMIPs (black line) and a slight increment in size, even not statistically significant (p value > 98%), upon fluorescent tagging both for Nile-Blue-bioMIPs (blue line) and Rhodamine BioMIPs (red line)

The requirements for selective recognition, high affinity, and non-toxicity were confirmed, in line with [11], thus the bioMIPs met the role of functional nanotraps for albumin.

With the aim to further exploit the bioMIPs for selective molecular nanotrapping *in vitro* and *in vivo*, we entailed fluorescent tags to the bioMIPs, so to enable their localization in tissues and cells through fluorescence microscopy techniques. For the labeling, the monomers Acryloxyethyl thiocarbamoyl rhodamine B and Nile-Blue Acrylamide were chosen. BioMIPs suspended in PBS at the estimated quantity of ~ 100 pmol were added of an excess ($\sim 600\times$ moles) of fluorescent monomers. The fluorescent tag decoration was performed via photocoupling with the biocompatible photoinitiator LAP. After the grafting, bioMIPs were extensively dialysed (15 kDa MWCO) to remove the non-reacted monomers. Tagging was proved by measuring the fluorescence emission of the bioMIPs prior and after tagging. Rhoda-bioMIPs and Nile-Blue-bioMIPs emitted, respectively, at 585 nm and at 685 nm, proving the effective tagging. The moles of fluorophore per mole of Rhoda-bioMIP particle were estimated to be 174 ± 16 . For Nile-Blue-bioMIPs, the moles of fluorophore were 98 ± 7 per mole of Nile-Blue-bioMIPs. The hydrodynamic size of the nanoparticles, monitored prior and after the tagging process (Fig. 2), showed bioMIPs ($Z_{\text{ave}} 95.6 \pm 1.2$ nm; PDI 0.358) underwent a slight increment in size upon tagging, displaying, respectively, $Z_{\text{ave}} = 98.9 \pm 0.8$ nm (PDI 0.457) for Nile Blue addition and $Z_{\text{ave}} = 100.9 \pm 0.7$ nm (PDI 0.464) for Rhodamine addition.

Localization of bioMIPs on cell cultures

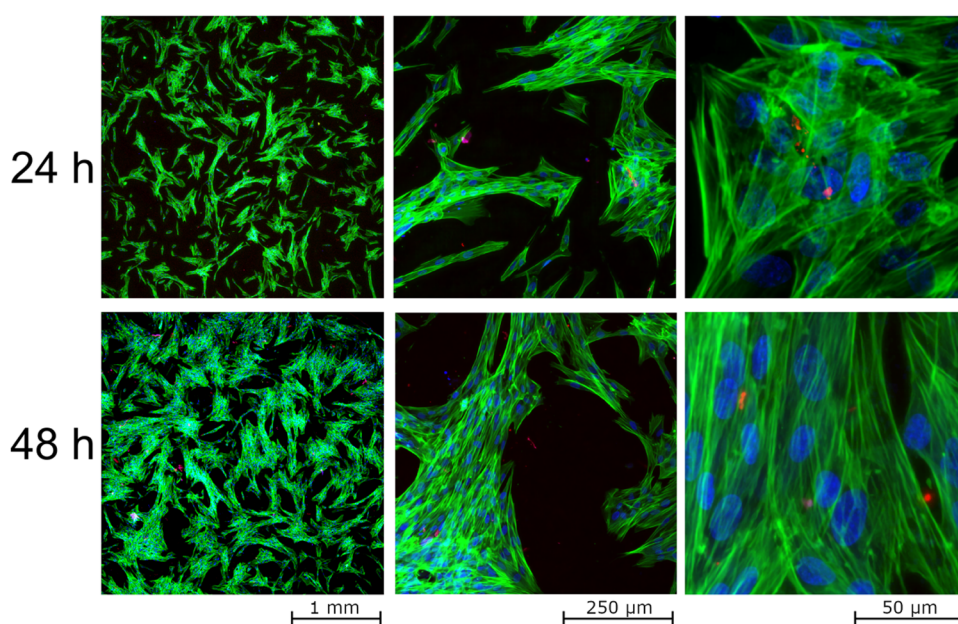
Next, we investigated the effect of the bioMIPs on cells cultures. SF bioMIPs were placed in contact with MRC5

cells (Fig. 3) as a model to evaluate their impact on living tissues. After 24 and 48 h of exposure to bioMIPs, at the concentration of 0.1 mg/mL, no significant impact on cell growth and proliferation was observed. Cell plates exposed to bioMIPs appeared equivalent to non-treated plates (Electronic Supplementary Materials, Figure S2), in full agreement with the preliminary cytotoxicity analysis reported in [11]. Fibroblasts maintained elongated shape, motility, and proliferation within the confined surface, confirming optimal conditions. In Fig. 3, bioMIPs, that are depicted as red spots, appear to accumulate as nanoparticles aggregates, mainly located in proximity of the cell nuclei, despite no internalization was further proved. Similar results were obtained at $5\times$ bioMIPs concentrations (0.5 mg/mL), as reported in the supplementary data (Fig. S3), which confirmed the safety of the SF bioMIP's formulation, in accordance with what reported for larger-scale SilMA scaffolds [13, 15, 16].

Biodegradation of bioMIPs

When considering the bioMIPs as molecular nanotraps for further therapeutic uses, the fate of these nanomaterials should be carefully studied. Here, we provided the first evidence on the degradation of the bioMIPs by enzymes. Both Rhoda- and Nile-Blue-bioMIPs were subjected to enzymatic degradation by using either the enzyme trypsin or Proteinase K. Trypsin is a human protease belonging to the class of the serine protease and characterized by a marked substrate specificity (cleaves the peptide bond at the C-term of lysines and arginines). Proteinase K is produced by the fungus *Engyodontium album* and belongs to the peptidase-S8 family. In contrast to trypsin, Proteinase K is characterized by an ample substrate specificity (cleaves the peptide

Fig. 3 Confocal pictures of MRC5 cells cytoskeleton and nuclei (green and blue, respectively) seeded on multi-well plate semi-confluence and exposed to 0.5 mg/mL bioMIPs solution (red) for 24 and 48 h. From left to right: $\times 4$, $\times 20$ and $\times 100$ magnification



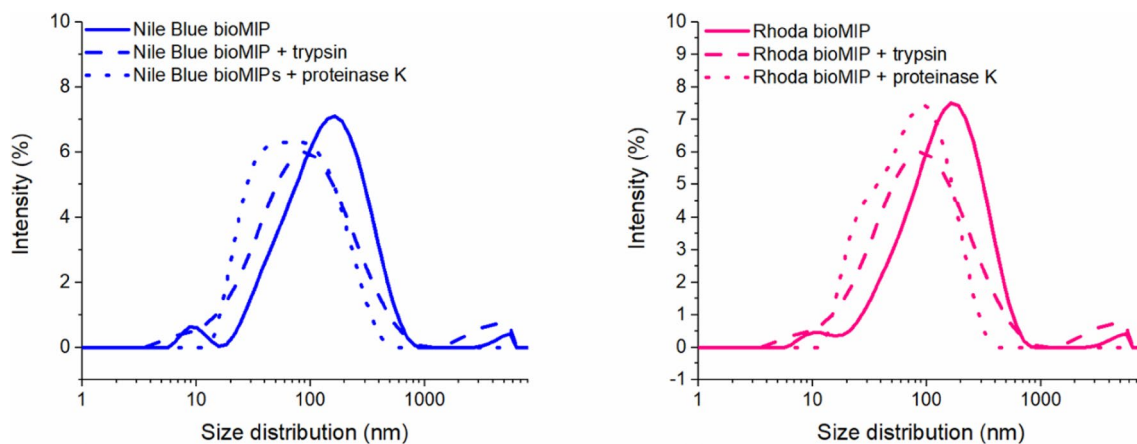


Fig. 4 Rhoda- and Nile Blue-bioMIP's degradations were followed at DLS. The mean hydrodynamic size of the bioMIPs decreased during the enzymatic digestion confirming the biodegradability of the nanotraps

bond at the C-term of aliphatic, aromatic, hydrophobic aminoacids). Prior to perform the wet experiment, an *in silico* prediction of the enzymatic cleavages (trypsin; Proteinase K) of SF was performed, using the tool Peptide Cutter of the ExPasy platform (web.expasy.org/cgi-bin/peptide_cutter/peptidecutter.pl). *In silico* results indicated Proteinase K can fully degrade SF into di-, tri-, and tetra-peptides (ESI for the full list of peptides), whereas trypsin just degrades SF in fewer peptides, generating few large macropptides and some ten peptides of 10–20 residues (details in ESI). It should be noted that *in silico* digestion was performed on SF heavy chain, whereas the bioMIPs are made of crosslinked SilMA, hence were considered a broad prediction.

The enzymatic degradations of bioMIPs were performed overnight at 37 °C and results were monitored at DLS (Fig. 4). Upon exposure to the enzymes, a significant reduction of the mean hydrodynamic size of the bioMIPs was observed, supporting the degradation of the nanoparticles. Digested bioMIPs were ultrafiltered on Amicon 10,000 Da MWCO, and the collected digestion products confirmed fluorescence emission.

Conclusions

BioMIPs are functional and non-toxic nanotraps, suitable for the selective recognition of a targeted analyte, thus meeting the conditions for the future clinical translation and the foreseen uses as therapeutics [11, 12]. Here, we demonstrated that bioMIPs can be post-synthetically decorated with fluorescent tags, so to enable their time and space-localization in cells cultures and tissues. Tested on human lung fibroblasts, the bioMIP's cell response was coherent with the results so far reported in the literature for methacrylated silk fibroin. Concerning the open question on the fate of such

nanomaterials *in vivo* and in the environment, the present results—despite preliminary—prove the possibility of biological activated degradation.

Supplementary Information The online version contains supplementary material available at <https://doi.org/10.1557/s43580-023-00507-3>.

Acknowledgments AMB thanks the Centro Piattaforme Tecnologiche (CPT), University of Verona for the use of the facility DLS.

Author contributions We confirm that the manuscript has been read and approved by all authors.

Funding Open access funding provided by Università degli Studi di Verona within the CRUI-CARE Agreement.

Declarations

Conflict of interest The authors declare no conflicts of interests.

Open Access This article is licensed under a Creative Commons Attribution 4.0 International License, which permits use, sharing, adaptation, distribution and reproduction in any medium or format, as long as you give appropriate credit to the original author(s) and the source, provide a link to the Creative Commons licence, and indicate if changes were made. The images or other third party material in this article are included in the article's Creative Commons licence, unless indicated otherwise in a credit line to the material. If material is not included in the article's Creative Commons licence and your intended use is not permitted by statutory regulation or exceeds the permitted use, you will need to obtain permission directly from the copyright holder. To view a copy of this licence, visit <http://creativecommons.org/licenses/by/4.0/>.

References

1. R. Arshady, K. Mosbach, *Die Makromol. Chemie* (1981). <https://doi.org/10.1002/macp.1981.021820240>

2. L. Cenci, R. Tatti, R. Tognato, E. Ambrosi, C. Piotta, A.M. Bossi, *Eur. Polym. J.* (2018). <https://doi.org/10.1016/J.EURPOLYMJ.2018.08.031>
3. Y. Hoshino, T. Kodama, Y. Okahata, K.J. Shea, *J. Am. Chem. Soc.* (2008). <https://doi.org/10.1021/ja8062875>
4. S. Ambrosini, S. Beyazit, K. Haupt, B. Tse Sum Bui, *Chem. Commun.* (2013). <https://doi.org/10.1039/c3cc41701h>
5. A. Poma, A.P.F. Turner, S.A. Piletsky, *Trends Biotechnol.* (2010). <https://doi.org/10.1016/j.tibtech.2010.08.006>
6. K. Haupt, *Nat. Mater.* (2010). <https://doi.org/10.1038/nmat2818>
7. A.M. Bossi, *Nat. Chem.* (2020). <https://doi.org/10.1038/s41557-019-0415-6>
8. Y. Dong, W. Li, Z. Gu, R. Xing, Y. Ma, Q. Zhang, Z. Liu, *Angew. Chemie Int. Ed.* (2019). <https://doi.org/10.1002/anie.201904860>
9. P.X. Medina Rangel, E. Moroni, F. Merlier, L.A. Gheber, R. Vago, B. Tse Sum Bui, K. Haupt, *Angew. Chemie Int. Ed.* (2020). <https://doi.org/10.1002/ange.201910373>
10. C. Boitard, A. Curcio, A.-L. Rollet, C. Wilhelm, C. Menager, N. Griffete, *A.C.S. Appl. Appl. Mater. Interfaces* (2019). <https://doi.org/10.1021/acsami.9b11717>
11. A.M. Bossi, A. Bucciarelli, D. Maniglio, *A.C.S. Appl. Mater. Interfaces* (2021). <https://doi.org/10.1021/acsami.1c05405>
12. A.M. Bossi, D. Maniglio, *Microchim. Acta* (2022). <https://doi.org/10.1007/s00604-022-05165-0>
13. A. Bucciarelli, T. Muthukumar, J.S. Kim, W.K. Kim, A. Quaranta, D. Maniglio, G. Khang, A. Motta, *A.C.S. Biomater. Sci. Eng.* (2019). <https://doi.org/10.1021/acsbiomaterials.9b00814>
14. D.N. Rockwood, R.C. Preda, T. Yücel, X. Wang, M.L. Lovett, D.L. Kaplan, *Nat. Protoc.* (2011). <https://doi.org/10.1038/nprot.2011.379>
15. S.H. Kim, Y.K. Yeon, J.M. Lee et al., *Nat. Commun.* (2018). <https://doi.org/10.1038/s41467-018-03759-y>
16. I.A. Barroso, K. Man, V.M. Villapun, S.C. Cox, A.K. Ghag, *ACS Biomater. Sci. Eng.* (2021). <https://doi.org/10.1021/acsbiomaterials.1c00791>

Publisher's Note Springer Nature remains neutral with regard to jurisdictional claims in published maps and institutional affiliations.